Journal of Computational Physics 345 (2017) 207–223

Contents lists available at ScienceDirect

Journal of Computational Physics

www.elsevier.com/locate/jcp

Functional level-set derivative for a polymer self consistent field theory Hamiltonian

Gaddiel Ouaknin [a,*], Nabil Laachi [e], Daniil Bochkov [a], Kris Delaney [e], Glenn H. Fredrickson [c,d,e], Frederic Gibou [a,b]

[a] Department of Mechanical Engineering, University of California, Santa Barbara, CA 93106-5070, USA
[b] Department of Computer Science, University of California, Santa Barbara, CA 93106-5110, USA
[c] Department of Chemical Engineering, University of California, Santa Barbara, CA 93106-5080, USA
[d] Department of Materials, University of California, Santa Barbara, CA 93106-5050, USA
[e] Materials Research Laboratory, University of California, Santa Barbara, CA 93106-5050, USA

ARTICLE INFO

Article history:
Received 20 January 2017
Received in revised form 12 April 2017
Accepted 18 May 2017
Available online 24 May 2017

Keywords:
SCFT
Level-set
Shape optimization
Block copolymer

ABSTRACT

We derive functional level-set derivatives for the Hamiltonian arising in self-consistent field theory, which are required to solve free boundary problems in the self-assembly of polymeric systems such as block copolymer melts. In particular, we consider Dirichlet, Neumann and Robin boundary conditions. We provide numerical examples that illustrate how these shape derivatives can be used to find equilibrium and metastable structures of block copolymer melts with a free surface in both two and three spatial dimensions.

1. Introduction

The use of polymers in confined domains is ubiquitous in science and engineering, ranging from novel lithography techniques at the sub 22-nanometer scale for next generation computer chips to the study of drug delivery carriers with controlled release to the study of thin films [15,17,16,18,36,35,14,26]. Self-consistent field theory (SCFT) provides an accurate description of the self-assembly of dense collections of long polymers at equilibrium by considering a Fokker–Planck equation that describes the probability of polymer segments to be at a certain spatial location and given chain contour length. This technique has been successfully used in the case of periodic as well as confined domains. The more difficult case of free boundaries is still in its infancy, although some authors have recently provided specialized solutions in the context of directed self-assembly, by considering a parametric description of the free boundary [20,19]. An important question in the context of free surfaces is how the self-assembled solution responds to a change in the free boundary's *shape*. Answering this question requires to either explicitly solve the direct problem several times in order to *a posteriori* estimate the sensitivity or to derive appropriate functional derivatives with respect to the level set to *a priori* estimate it. The advantage of an *a priori* approach is that it enables the development and implementation of algorithms that optimize the shape.

Shape derivatives have been derived for many systems described by partial differential equations with various boundary conditions; a rigorous derivation of the methods and examples can be found in the seminal book of Sokolowski and Zolesio

* Corresponding author.
E-mail address: gaddielouaknin@umail.ucsb.edu (G. Ouaknin).

http://dx.doi.org/10.1016/j.jcp.2017.05.037
0021-9991/

[39] and the more recent book of Delfour and Zolesio [8]. The level-set framework introduced by Osher and Sethian [28] which uses a scalar function to implicitly represent any arbitrary shape, has been implemented to study shape optimization for a variety of physical applications such as structural optimization, tomography and inverse obstacle problems in fluids, among others [29,3,1,41,5,6].

On the other hand, functional shape derivatives in the context of SCFT have only been derived for orthorhombic shapes [2]. In the present, we derive functional shape derivatives with arbitrary shapes using the level-set description recently proposed by Ouaknin et al. [31,30]. In [31], the authors showed that the use of Neumann boundary conditions, as modeled by deGennes [7], is needed in order to robustly evaluate physical quantities at the free boundary. In [30], they use that framework in the context of directed self-assembly to propose an algorithm that will find the geometry of a mask that will guide the self-assembly of block-copolymers to a target configuration. For this purpose, they chose a physically intuitive velocity for the level set function by taking it equal to the pressure field. In the present work we do not search for a shape that will result in a desired self assembly, which is the focus of [31]; instead we search for the shape that will result in the *minimum free energy*, without considering a target. In addition we do not define the velocity to be the pressure field but derive and use the rigorous functional level set derivative of the free energy.

The paper is structured as follows: in section 2 we present the SCFT equations, in section 3 we derive functional level-set derivatives for SCFT for various boundary conditions and in section 4 we present examples of shape optimization using these level-set derivatives in both two and three spatial dimensions.

2. Self-consistent field theory model

In this section, we describe the governing equations for self-consistent field theory [9,11,12,21] in the context of an incompressible melt of diblock copolymers composed of two monomer species A and B. This physical system is characterized by two parameters: (1) f_A, the fraction of block A and (2) χ_{AB}, the repulsion interaction between A and B polymer segments. The field-based theory of polymer thermodynamics uses a Hubbard–Stratonovich transform to convert the partition function from a particles representation to a field representation. If one further imposes the mean-field, or self-consistent field, approximation, the SCFT equations are obtained by finding for the statistical fields w_- (the exchange field) and w_+ (the pressure field) that optimize the free energy, i.e. the Hamiltonian[1]:

$$H[w_+, w_-] = \frac{1}{V}\int_\Omega \Big(- w_+(\boldsymbol{r}) + \frac{w_-^2(\boldsymbol{r})}{\chi_{AB}}\Big)\, d\boldsymbol{r} - \ln Q\,[w_+(\boldsymbol{r}), w_-(\boldsymbol{r})], \tag{1}$$

where the normalized partition function Q can be formulated as:

$$Q\,[w_+, w_-] = \frac{1}{V}\int_\Omega q(s=1, \boldsymbol{r}; [w_+(\boldsymbol{r}), w_-(\boldsymbol{r})])\, d\boldsymbol{r},$$

where Ω is the domain considered and V its volume. In these equations, $w_+(\boldsymbol{r})$ acts as a pressure potential that enforces the incompressibility constraint while the exchange potential, $w_-(\boldsymbol{r})$, describes the interaction between A and B. The functionals $q(s, \boldsymbol{r}; [w_+, w_-])$ and $q^\dagger(s, \boldsymbol{r}; [w_+, w_-])$ are the solution of a Fokker Planck equation, which has to be solved from $s = 0$ to $s = 1$, with initial conditions $q(s = 0, \boldsymbol{r}) = q^\dagger(s = 0, \boldsymbol{r}) = 1$, where s is the contour of a polymer chain. The functionals q and $q^\dagger$, called the chain propagators, represent the statistical weight of piece of chain at location $\boldsymbol{r}$ and contour length s and satisfy the following forward and backward Fokker–Planck equations:

$$\begin{cases} \partial_s q(s, \boldsymbol{r}) = \Delta q(s, \boldsymbol{r}) - q(s, \boldsymbol{r})\, w(s, \boldsymbol{r}) & \text{forward,} \\ \partial_s q^\dagger(s, \boldsymbol{r}) = \Delta q^\dagger(s, \boldsymbol{r}) - q^\dagger(s, \boldsymbol{r})\, w^\dagger(\boldsymbol{r}, s) & \text{backward,} \end{cases} \tag{2}$$

where the forward potential $w(s, \boldsymbol{r})$ and the backward potential $w^\dagger(s, \boldsymbol{r}) = w(1 - s, \boldsymbol{r})$ depend on $w_+(\boldsymbol{r})$ and $w_-(\boldsymbol{r})$ as defined next in equation (3). The uniform initial condition $q(s = 0, \boldsymbol{r}) = 1$ is interpreted as an uniform spatial probability for the polymer chain's initial location $s = 0$, i.e. the free end of the polymer chain. The Fokker–Planck equation for q describes a random walk of a polymer chain interacting with an external potential $w(\boldsymbol{r}, s)$, where $q(s, \boldsymbol{r})$ is proportional to the probability of the polymer chain to be at location $\boldsymbol{r}$ for a given contour length s. The Fokker–Planck equation for $q^\dagger(s, \boldsymbol{r})$ describes the case where the second free end of the polymer chain has a uniform spatial probability, since $w^\dagger(s, \boldsymbol{r}) = w(1 - s, \boldsymbol{r})$ and $q^\dagger(s = 0, \boldsymbol{r}) = 1$.

The essence of the boundary conditions that we detail next is directly related to the probability of the polymeric material to be at the free boundary $\Gamma = \partial\Omega$. Specifically, the boundary conditions at the free boundary that we consider in this study are:

[1] This is actually H/n, where n is the number of molecular chains. Likewise χ_{AB} is in fact $\chi_{AB}N$ where N is the number of molecular segments per chain.

1. Homogeneous Dirichlet:

$$q(s,\boldsymbol{r}) = 0 \quad \text{and} \quad q^\dagger(s,\boldsymbol{r}) = 0.$$

2. Homogeneous Neumann:

$$\frac{\partial q(s,\boldsymbol{r})}{\partial \boldsymbol{n}} = 0 \quad \text{and} \quad \frac{\partial q^\dagger(s,\boldsymbol{r})}{\partial \boldsymbol{n}} = 0.$$

3. Homogeneous Robin:

$$q(s,\boldsymbol{r}) + \alpha_A \frac{\partial q(s,\boldsymbol{r})}{\partial \boldsymbol{n}} = 0, \quad \text{for } 0 < s < f_A \qquad \text{and} \quad q(s,\boldsymbol{r}) + \alpha_B \frac{\partial q(s,\boldsymbol{r})}{\partial \boldsymbol{n}} = 0, \quad \text{for } f_A < s < 1,$$

$$q^\dagger(s,\boldsymbol{r}) + \alpha_B \frac{\partial q^\dagger(s,\boldsymbol{r})}{\partial \boldsymbol{n}} = 0, \quad \text{for } 0 < s < 1 - f_A \quad \text{and} \quad q^\dagger(s,\boldsymbol{r}) + \alpha_A \frac{\partial q^\dagger(s,\boldsymbol{r})}{\partial \boldsymbol{n}} = 0, \quad \text{for } 1 - f_A < s < 1,$$

where we can denote $\alpha(s)$ for α_A or α_B in the Robin boundary condition for q and $q^\dagger$ which describe the attraction or the repulsion from the wall for the A and B species [9]. The forward potential $w(\boldsymbol{s},\boldsymbol{r})$ is calculated as follows:

$$w(s,\boldsymbol{r}) = \begin{cases} w_A(\boldsymbol{r}) = w_+(\boldsymbol{r}) - w_-(\boldsymbol{r}) & 0 < s < f_A \\ w_B(\boldsymbol{r}) = w_+(\boldsymbol{r}) + w_-(\boldsymbol{r}) & f_A < s < 1 \end{cases}, \tag{3}$$

and $w^\dagger(s,\boldsymbol{r}) = w(1-s,\boldsymbol{r})$. The normalized densities of the components A and B, $\rho_A(\boldsymbol{r}), \rho_B(\boldsymbol{r})$ are obtained through the functional derivatives with respect to $w_A(\boldsymbol{r})$ and $w_B(\boldsymbol{r})$, $\frac{\delta H}{\delta w_A(\boldsymbol{r})}, \frac{\delta H}{\delta w_B(\boldsymbol{r})}$ and are computed using q and $q^\dagger$:

$$\rho_A(\boldsymbol{r};[w_+,w_-]) = \frac{1}{Q[w_+,w_-]} \int_0^{f_A} q^\dagger(1-s,\boldsymbol{r},[w_+,w_-]) q(s,\boldsymbol{r},[w_+,w_-])\, ds,$$

$$\rho_B(\boldsymbol{r};[w_+,w_-]) = \frac{1}{Q[w_+,w_-]} \int_{f_A}^{1} q^\dagger(1-s,\boldsymbol{r},[w_+,w_-]) q(s,\boldsymbol{r},[w_+,w_-])\, ds.$$

In the mean-field or SCFT approximation, where fluctuations are neglected, the free energy of the melt is then given by the Hamiltonian at the saddle point, i.e. when $\frac{\delta H}{\delta w_-(\boldsymbol{r})} = \frac{\delta H}{\delta w_+(\boldsymbol{r})} = 0$. The forces of the optimization process, $f_+(\boldsymbol{r})$, the pressure force and $f_-(\boldsymbol{r})$ the exchange force, are obtained through the functional derivatives with respect to the statistical fields, $\frac{\delta H}{\delta w_+(\boldsymbol{r})}, \frac{\delta H}{\delta w_-(\boldsymbol{r})}$, and are given by:

$$\begin{cases} f_+(\boldsymbol{r}) &= \rho_A(\boldsymbol{r}) + \rho_B(\boldsymbol{r}) - 1 \\ f_-(\boldsymbol{r}) &= \dfrac{2w_-(\boldsymbol{r})}{\chi_{AB}} + \rho_B(\boldsymbol{r}) - \rho_A(\boldsymbol{r}) \end{cases}. \tag{4}$$

3. Shape derivative for SCFT

3.1. Overview

We first formulate the optimization problem and then recall some of the main results of shape optimization theory. The shape optimization can be cast into the following formulation:

$$\text{minimize}_\Omega H(\Omega) := \frac{1}{|\Omega|} \int_\Omega f(\boldsymbol{r},\Omega)\, d\boldsymbol{r} - \log\left(\frac{1}{|\Omega|} \int_\Omega q(\boldsymbol{r},\Omega)\, d\boldsymbol{r} \right),$$

where the two functions $f(\boldsymbol{r},\Omega)$ and $q(\boldsymbol{r},\Omega)$ are given by the SCFT algorithms. If the volume $|\Omega|$ is to be preserved, the minimization can be formulated as the constrained minimization:

$$\text{minimize}_\Omega H(\Omega) := \frac{1}{|\Omega|} \int_\Omega f(\boldsymbol{r},\Omega)\, d\boldsymbol{r} - \log\left(\int_\Omega q(\boldsymbol{r},\Omega)\, d\boldsymbol{r} \right), \text{ subject to } |\Omega| = V.$$

As we will see in the Lagrangian approach next, the augmented Lagrangian method splits the constrained minimization into several simple steps. One of the main steps is to minimize $H(\Omega)$ over Ω while f and q are fixed, ignoring their dependences on Ω. This step can be solved by evolving Ω with the normal velocity, simply given as

$$v_n = \frac{1}{|\Omega|} f - \frac{q}{\int_\Omega q\, dx} \text{ on } \Gamma.$$

Bregman iteration and operator splitting methods can also be applied [11]. We now recap the main results of shape derivative theory and introduce the level set representation of shapes. In 3.2 we present the Lagrangian approach to shape derivatives known as Cea's method, in 3.3 we derive the shape derivative of H with a Lagrangian approach and with a level set approach.

The Hamiltonian as described in the previous section is a function of the domain Ω in addition of the statistical fields: $H = H[w_+, w_-, \Omega]$, where $w_+, w_- : \Omega \mapsto R$ are smooth enough functions and $\Omega \in \aleph$ where $\aleph = \{\Omega : \Omega \subset \boldsymbol{R}^d\}$ with $d = 2, 3$ for two and three spatial dimension problems respectively. H is a functional smooth enough $R^d \times R^d \times R^d \mapsto R$ and in the case of a variable shape $H = H[w_+, w_-, \Omega_t]$ with $\Omega_t \in \aleph$. The family of perturbed domains $\Omega_t = T_t(\boldsymbol{v}, \Omega) = \{T_t(\boldsymbol{v}, \boldsymbol{r}) : \boldsymbol{r} \in \Omega\}$ is the result of the flow equation $T_t(\boldsymbol{v}, \boldsymbol{r}) = \boldsymbol{r} + t\boldsymbol{v}$. We are interested to compute $dH[\Omega, \boldsymbol{v}] = \lim_{t\to 0} \frac{H[w_+, w_-, \Omega_t] - H[w_+, w_-, \Omega_0]}{t}$.

We recall main results from Sokolowski and Zolesio [39] and Delfour and Zolesio [8]. These formulas can be found in [39] page 113 equation (2.168), page 116 equation (2.174) and (3.42) page 481, (4.7) page 484, (4.17) page 486 in [8]. For a smooth function $f(\boldsymbol{r}) : \Omega \mapsto R$, non-related to a state equation we define the following domain functional, $J_1[f(\boldsymbol{r}); \Omega] = \int_\Omega f(\boldsymbol{r}) d\boldsymbol{r}$, defined in Ω. Given a continuous velocity field $\boldsymbol{v}(t, \boldsymbol{r})$ with normal velocity at v_n at $t = 0$, the corresponding shape derivative of the functional is given by:

$$dJ_1[f(\boldsymbol{r}); \Omega; v_n] = \int_\Gamma f(\boldsymbol{r}) v_n d\Gamma,$$

where the integral over Γ is over the original shape's boundary (unchanged).

We can also consider a functional of a sufficiently smooth boundary $\Gamma := \partial\Omega$, $J_2[f(\boldsymbol{r}), \Omega] = \int_\Gamma f(\boldsymbol{r}) d\Gamma$, the corresponding shape derivative of the functional is given by:

$$dJ_2[f(\boldsymbol{r}); \Omega; v_n] = \int_\Gamma \Big(\frac{\partial f(\boldsymbol{r})}{\partial \boldsymbol{n}}\Big|_\Gamma + \kappa(\boldsymbol{r}) f(\boldsymbol{r}) \Big) \boldsymbol{v}_n(\boldsymbol{r}) d\Gamma,$$

where $\kappa(\boldsymbol{r})$ is the curvature of Γ and the integral over Γ is over the original boundary shape (unperturbed).

When a functional J depends on a function u which depends on a state equation $E(u, \Omega) = 0$ we must add a term for u' as below [39]. Alternatively we can use the above formulas and use a Lagrangian formulation where the state equation is combined with the cost function through a Lagrange multiplier [4] (and chapter 10.5 in [8] for a rigorous treatment and conditions of the Lagrangian approach) as we will see next in section 3.2. We now rewrite the formulas with u' where u, u' are smooth enough. For a functional, $J_3[u(\boldsymbol{r}); \Omega] = \int_\Omega u(\boldsymbol{r}) d\boldsymbol{r}$, defined in Ω, and given $\boldsymbol{v}(t, \boldsymbol{r})$ with normal velocity v_n at $t = 0$, the corresponding change of the functional is given by:

$$dJ_3[u(\boldsymbol{r}); \Omega; v_n] = \int_\Omega u'(\boldsymbol{r}, [\Omega; v_n]) d\boldsymbol{r} + \int_\Gamma u(\boldsymbol{r}, [\Omega; v_n]) v_n d\Gamma.$$

Next considering a functional, $J_4[u(\boldsymbol{r})] = \int_\Gamma u(\boldsymbol{r}) d\Gamma$, defined on $\Gamma = \partial\Omega$ with u, u' smooth enough on Γ the corresponding change of the functional is given by:

$$dJ_4[u(\boldsymbol{r}); \Omega; v_n] = \int_\Gamma u'(\boldsymbol{r})\Big|_\Gamma d\Gamma + \int_\Gamma \Big(\frac{\partial u(\boldsymbol{r})}{\partial \boldsymbol{n}}\Big|_\Gamma + \kappa(\boldsymbol{r}) u(\boldsymbol{r}) \Big) v_n(\boldsymbol{r}) d\Gamma.$$

In addition the following formula for integrating by parts on the surface Γ is useful. For f and g smooth enough (proposition 2.67 in page 93 of [39]):

$$\int_\Gamma \nabla f(\boldsymbol{r}) \cdot \nabla g(\boldsymbol{r}) d\Gamma = \int_\Gamma -f(\boldsymbol{r}) \cdot \Delta g(\boldsymbol{r}) d\Gamma + \int_\Gamma [\frac{\partial f(\boldsymbol{r})}{\partial \boldsymbol{n}} \frac{\partial g(\boldsymbol{r})}{\partial \boldsymbol{n}} + f(\boldsymbol{r}) \frac{\partial^2 g(\boldsymbol{r})}{\partial \boldsymbol{n}^2} + \kappa(\boldsymbol{r}) f(\boldsymbol{r}) \frac{\partial g(\boldsymbol{r})}{\partial \boldsymbol{n}}] d\Gamma.$$

In this work, the shape is described through a level-set function, $\phi(\boldsymbol{r})$, which describes an irregular domain, Ω, in an implicit way (see Fig. 1): $\phi(\boldsymbol{r})$ is negative inside Ω, positive outside, and zero at its boundary Γ. The Fokker–Planck equations

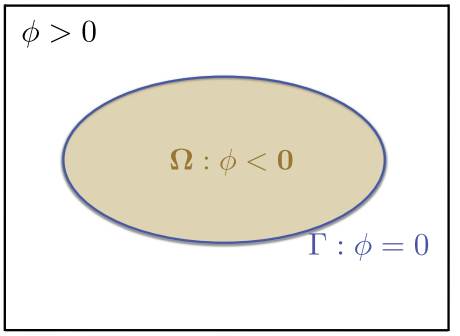

Fig. 1. Level-set representation of an irregular domain Ω with boundary Γ.

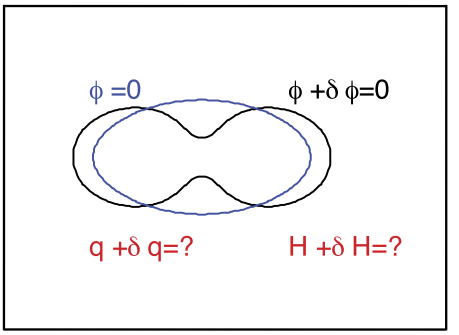

Fig. 2. Schematic illustrating how $q(\boldsymbol{r}, s)$, the solution of $\partial_s q = \nabla^2 q - wq$, varies to $q + \delta q$, and by consequence how the free energy H varies to $H + \delta H$, as the shape is perturbed from ϕ to $\phi + \delta\phi$.

are thus solved in Ω where $\phi < 0$ with the boundary conditions imposed at the interface Γ, where $\phi(\boldsymbol{r}) = 0$. The volume of the polymer V is equal to $|\Omega| = \int \mathcal{H}(-\phi(\boldsymbol{r}))d\boldsymbol{r}$ where $\mathcal{H}$ is the Heaviside function. In this study we choose $\phi(\boldsymbol{r})$ to be a signed distance function, i.e. $|\nabla\phi(\boldsymbol{r})| = 1$. The outward normal to Ω is thus defined as $\boldsymbol{n} = \nabla\phi(\boldsymbol{r})$, the local mean curvature is $\kappa(\boldsymbol{r}) = \nabla \cdot \nabla\phi(\boldsymbol{r})$ and $\dfrac{\partial q(\boldsymbol{r})}{\partial \boldsymbol{n}} = \nabla q \cdot \nabla\phi$.

With such a representation, the Hamiltonian is a functional of $\phi(\boldsymbol{r})$, in addition to the pressure field $w_+(\boldsymbol{r})$ and the exchange field $w_-(\boldsymbol{r})$; thus one writes $H = H[w_+, w_-, \phi]$. To quantify how the Hamiltonian H responds to a change in the irregular domain's shape, we need to find how Q changes and in turn how the chain propagators $q(s = 1, \boldsymbol{r})$ and $q^\dagger(s = 1, \boldsymbol{r})$ vary. The change in the shape is expressed through a perturbation of the interface Γ via the level-set function $\phi(\boldsymbol{r}) \to \phi(\boldsymbol{r}) + \delta\phi(\boldsymbol{r})$ (see Fig. 2). In turn we need to find how $q(s = 1, \boldsymbol{r}) \to q(s = 1, \boldsymbol{r}) + \delta q(s = 1, \boldsymbol{r})$ and $q^\dagger(s = 1, \boldsymbol{r}) \to q^\dagger(s = 1, \boldsymbol{r}) + \delta q^\dagger(s = 1, \boldsymbol{r})$.

The formulas stated before can be rewritten when $\delta\phi = -v_n dt$, $dJdt = \delta J, u'dt = \delta u$: for $J[u(\boldsymbol{r})] = \int_\Omega u(\boldsymbol{r})d\boldsymbol{r}$, defined in Ω, given a change $\delta\phi(\boldsymbol{r})$ of the shape, the corresponding change of the functional is given by:

$$\delta J[u(\boldsymbol{r})] = \int_\Omega \delta u(\boldsymbol{r})d\boldsymbol{r} - \int_\Gamma u(\boldsymbol{r})\delta\phi(\boldsymbol{r})d\Gamma,$$

and for a functional $J[u(\Gamma)] = \int_\Gamma u(\Gamma)d\Gamma$, defined on Γ with $u(\Gamma) = u(\boldsymbol{r})\Big|_\Gamma$, given a change $\delta\phi(\boldsymbol{r})$ of the shape, the change of the functional is given by:

$$\delta J(u) = \int_\Gamma \delta u(\boldsymbol{r})\Big|_\Gamma d\Gamma - \int_\Gamma \left(\frac{\partial u(\boldsymbol{r})}{\partial \boldsymbol{n}}\Big|_\Gamma + \kappa(\boldsymbol{r})u(\boldsymbol{r})\right)\delta\phi(\boldsymbol{r})d\Gamma.$$

3.2. Lagrangian approach

In [4], Cea introduced a method based on a Lagrangian functional to calculate the shape derivative of a functional $J[u, \phi] = \int_\Omega u(\boldsymbol{r})d\Omega$, where $u(\boldsymbol{r})$ is the solution of a partial differential equation $E(\phi(\boldsymbol{r}), u(\boldsymbol{r})) = 0.$, with $\Omega = \{\boldsymbol{r} : \phi(\boldsymbol{r}) < 0\}$. and $\phi(\boldsymbol{r})$ is a level-set function. To find the change of J with respect to ϕ one introduces the Lagrangian $L[u, \phi, \lambda] = J[u, \phi] + \int_\Omega \lambda(\boldsymbol{r})E(\phi, u)d\Omega$. We highlight the steps of the derivation used by [4]:

1. Since $\delta L_{\delta\lambda} = \int_\Omega \delta\lambda E(\phi,u)d\Omega$ and $E(\phi,u)=0$, u is the solution of $\delta L_{\delta\lambda}=0$.
2. Since we choose λ to be the solution of $\delta L_{\delta u}=0$, λ satisfies $\delta J_{\delta u} + \int_\Omega \lambda(\boldsymbol{r})\delta E_{\delta u}(\phi,u)d\Omega = 0$.
3. When the constraint $E(u,\phi)=0$ is satisfied we can write $j[u,\phi,\lambda] = L[u,\phi,\lambda]$ so that the change of $j[u,\phi,\lambda]$ with respect to the shape is given by: $\delta j_{\delta\phi} = \delta L_{\delta\phi} + \delta L_{\delta u}\delta u_{\delta\phi} + \delta L_{\delta\lambda}\delta\lambda_{\delta\phi} = \delta L_{\delta\phi}$.
4. Finally Hadamard's theorem states that the change of a functional $j[u]$ with respect to the shape depends on the values on Γ only [13], thus:

$$\delta j_{\delta\phi} = -\int_\Gamma \Big(u(\boldsymbol{r}) + \lambda(\boldsymbol{r})E(\phi(\boldsymbol{r}),u(\boldsymbol{r}))\Big)\delta\phi(\boldsymbol{r})d\Gamma.$$

We note that the method of Cea needs to be used with certain precautions [32] and chapter 10.5 in [8]. More recently Sturm [40] proposed a simple test for the Cea method. The formula for $\delta j_{\delta\phi}$ is obtained assuming u', λ' are integrable which may leads to the incorrect formula. Instead $\delta j_{\delta\phi}$ should be rewritten when δu is rewritten as $\dot{u}dt$ instead of $u'dt$. When u' is for the shape derivative and $\dot{u}$ is for the material derivative [39]. Then the relation between u' and $\dot{u}$ is recalled as $u' = \dot{u} - \nabla u\cdot\boldsymbol{v}$ and $\lambda' = \dot{\lambda} - \nabla\lambda\cdot\boldsymbol{v}$ with $\dot{u},\dot{\lambda}$ integrable such that $\delta j_{\delta\phi} = \delta L_{\delta\phi} - \delta L_{\delta u}\nabla u\cdot\boldsymbol{v} + \delta L_{\delta\lambda}\nabla\lambda\cdot\boldsymbol{v}$. Since in our case that there are no spatial discontinuities $\delta L_{\delta u}\nabla u\cdot\boldsymbol{v} + \delta L_{\delta\lambda}\nabla\lambda\cdot\boldsymbol{v} = 0$ and $\delta j_{\delta\phi} = \delta L_{\delta\phi}$ and thus we can safely use the Cea method.

3.3. Shape derivatives for the Hamiltonian H

Considering shape optimization in the context of self-consistent field theory is complicated by the fact that the functional H not only depends on ϕ but also on the fields $w_+(\boldsymbol{r})$ and $w_-(\boldsymbol{r})$. We thus have:

$$\delta H = \int_\Omega [\frac{\delta H}{\delta\phi(\boldsymbol{r})}\delta\phi(\boldsymbol{r}) + \frac{\delta H}{\delta w_+(\boldsymbol{r})}\delta w_+(\boldsymbol{r}) + \frac{\delta H}{\delta w_-(\boldsymbol{r})}\delta w_-(\boldsymbol{r})]d\boldsymbol{r}.$$

Section 2 provides expressions for $\frac{\delta H}{\delta w_+(\boldsymbol{r})}$ and $\frac{\delta H}{\delta w_-(\boldsymbol{r})}$. In what follows, we denote

$$\delta H_{\delta\phi} = H[\phi+\delta\phi, w_+, w_-] - H[\phi, w_+, w_-] = \int_\Omega \frac{\delta H}{\delta\phi(\boldsymbol{r})}\delta\phi(\boldsymbol{r})d\boldsymbol{r}$$

and derive expressions for $\frac{\delta H}{\delta\phi(\boldsymbol{r})}$.

Now writing $\delta \ln Q = \frac{1}{Q}\delta Q$ term in equation (1) for the Hamiltonian, we have:

$$\delta H_{\delta\phi} = -\frac{1}{V}\int_\Gamma \Big(-w_+(\boldsymbol{r}) + \frac{w_-(\boldsymbol{r})^2}{\chi_{AB}}\Big)\delta\phi(\boldsymbol{r})\,d\Gamma - \frac{1}{Q}\delta Q_{\delta\phi} - \frac{\delta V_{\delta\phi}}{V^2}\int_\Omega \Big(-w_+(\boldsymbol{r}) + \frac{w_-^2(\boldsymbol{r})}{\chi_{AB}}\Big)d\boldsymbol{r} - \frac{-\delta V_{\delta\phi}}{V^2}Q, \quad (5)$$

where the fields $w_+(\boldsymbol{r})$ and $w_-(\boldsymbol{r})$ are kept constant. In the case of a fixed amount of incompressible polymeric material, hence a fixed volume $V = |\Omega| = \text{constant}$, we have $\delta V_{\delta\phi} = 0$. Therefore the expression for $\delta H_{\delta\phi}$ simplifies to:

$$\delta H_{\delta\phi} = -\frac{1}{V}\int_\Gamma \Big(-w_+(\boldsymbol{r}) + \frac{w_-(\boldsymbol{r})^2}{\chi_{AB}}\Big)\delta\phi(\boldsymbol{r})\,d\Gamma - \frac{1}{Q}\delta Q_{\delta\phi}. \quad (6)$$

The term $\delta Q_{\delta\phi}$ requires one to take into account the change in the solution of the Fokker–Planck equation and the associated boundary conditions. In the following derivations we are going to treat the term $\delta Q_{\delta\phi}$ only which can be reintroduced in (6), and we note that all the other terms do not have a dependence on $q(\boldsymbol{r},s)$.

To find $\delta Q_{\delta\phi}$ with a Lagrangian approach we define:

$$L = \int_{\Omega\times[0,1]} q(s,\boldsymbol{r})\delta(s=1)\,ds\,d\Omega$$
$$+ \int_{\Omega\times[0,1]} \lambda(s,\boldsymbol{r})\Big(q_s(s,\boldsymbol{r}) - \big[\Delta q(s,\boldsymbol{r}) - q(s,\boldsymbol{r})\,w(s,\boldsymbol{r})\big]\Big)\,ds\,d\Omega,$$

where $\lambda(s,\boldsymbol{r})$ is a Lagrange multiplier to enforce the Fokker–Planck equation (2) for q in Ω. After integrating by part the Lagrangian can be rewritten as:

$$\begin{aligned} L = & \int\limits_{\Omega\times[0,1]} q(s,\boldsymbol{r})\delta(s=1)\; ds\, d\Omega \\ & + \int\limits_{\Omega\times[0,1]} \lambda(s,\boldsymbol{r})\Big(q_s(s,\boldsymbol{r}) + q(s,\boldsymbol{r})\, w(s,\boldsymbol{r})\Big) + \nabla q(s,\boldsymbol{r})\cdot\nabla\lambda(s,\boldsymbol{r})\; ds\, d\Omega \\ & - \int\limits_{\Gamma\times[0,1]} \lambda(s,\boldsymbol{r})\frac{\partial q(s,\boldsymbol{r})}{\partial \boldsymbol{n}}\; d\Gamma\, ds, \end{aligned}$$

and after inserting the Robin boundary conditions of q on Γ:

$$\begin{aligned} L = & \int\limits_{\Omega\times[0,1]} q(s,\boldsymbol{r})\delta(s=1)\; ds\, d\Omega \\ & + \int\limits_{\Omega\times[0,1]} \lambda(s,\boldsymbol{r})\Big(q_s(s,\boldsymbol{r}) + q(s,\boldsymbol{r})\, w(s,\boldsymbol{r})\Big) + \nabla q(s,\boldsymbol{r})\cdot\nabla\lambda\; ds\, d\Omega \\ & + \int\limits_{\Gamma\times[0,1]} \lambda(s,\boldsymbol{r})\alpha(s) q(s,\boldsymbol{r})\; d\Gamma\, ds. \end{aligned}$$

- The change of L in response to a change in δq is:

$$\begin{aligned} \delta L_{\delta q} = & \int\limits_{\Omega\times[0,1]} \delta q(s,\boldsymbol{r})\delta(s=1)\; ds\, d\Omega \\ & + \int\limits_{\Omega\times[0,1]} \lambda(s,\boldsymbol{r})\Big(\delta q_s(s,\boldsymbol{r}) + \delta q(s,\boldsymbol{r})\, w(s,\boldsymbol{r})\Big) + \nabla\delta q(s,\boldsymbol{r})\cdot\nabla\lambda(s,\boldsymbol{r})\; ds\, d\Omega \\ & + \int\limits_{\Gamma\times[0,1]} \lambda(s,\boldsymbol{r})\alpha(s)\delta q(s,\boldsymbol{r})\; d\Gamma\, ds. \end{aligned} \tag{7}$$

Integrating by parts in space, we obtain:

$$\int\limits_{\Omega} \lambda\Delta\delta q\; d\Omega = \int\limits_{\Omega} \Delta\lambda\delta q\; d\Omega + \int\limits_{\Gamma} \lambda\frac{\partial\delta q}{\partial\boldsymbol{n}}\; d\Gamma - \int\limits_{\Gamma} \delta q\frac{\partial\lambda}{\partial\boldsymbol{n}}\; d\Gamma. \tag{8}$$

Likewise, integrating by parts in the chain contour variable gives:

$$\int\limits_{0}^{1} \lambda\delta q_s\; ds = -\int\limits_{0}^{1} \lambda_s\delta q\; ds + [\lambda\delta q]_0^1,$$

with

$$[\lambda\delta q]_{s=0}^{s=1} = \lambda(s=1)\delta q(s=1) - \lambda(s=0)\delta q(s=0),$$

where the second term drops out since $\delta q(s=0)=0$. Finally, with the change of variable $s=1-t$, we have:

$$\int\limits_{0}^{1} \lambda\delta q_s ds = \int\limits_{0}^{1} \lambda_t\delta q\; dt + \lambda(s=1)\delta q(s=1) \quad \text{and} \quad w(t) = w(1-s) = w^{\dagger}(s) \quad \text{and} \quad \alpha(t) = \alpha(1-s) = \alpha^{\dagger}(s). \tag{9}$$

Combining equations (7)–(9), we have:

$$\delta L_{\delta q} = \int_{\Omega\times[0,1]} \Big(1+\lambda(t,\boldsymbol{r})\Big)\delta(t=0)\delta q + \Big(\lambda_t(t,\boldsymbol{r}) - \Delta\lambda(t,\boldsymbol{r}) + \lambda(t,\boldsymbol{r})w^\dagger\Big)\delta q(s,\boldsymbol{r})\, d\Omega\, dt$$
$$+ \int_{\Gamma\times[0,1]} \lambda(t,\boldsymbol{r})\alpha^\dagger(s)\delta q(s,\boldsymbol{r}) + \delta q(s,\boldsymbol{r})\frac{\partial\lambda(t,\boldsymbol{r})}{\partial \boldsymbol{n}}\, d\Gamma\, dt,$$

and following Cea, we require the change in q to be zero to obtain the following system of equations for λ:

$$\begin{cases} \lambda_t(t,\boldsymbol{r}) = \Delta\lambda(t,\boldsymbol{r}) - \lambda(t,\boldsymbol{r})\, w^\dagger(t,\boldsymbol{r}) \text{ in } \Omega. \\ \lambda(t,\boldsymbol{r})\alpha^\dagger(t) + \dfrac{\partial\lambda(t,\boldsymbol{r})}{\partial\boldsymbol{n}} = 0 \text{ on } \Gamma. \\ \lambda(t=0,\boldsymbol{r}) = -1 \text{ in } \Omega. \end{cases} \tag{10}$$

Also comparing with equation (2), we have $\lambda = -q^\dagger$.

- The change of L in response to a change in $\delta\phi$ is:

$$\delta L_{\delta\phi} = -\int_{\Gamma\times T} q(s,\boldsymbol{r})\delta(s=1)\delta\phi\, ds\, d\Gamma$$
$$-\int_{\Gamma\times T} \Big(\lambda(1-s,\boldsymbol{r})\Big(q_s(s,\boldsymbol{r}) + q(s,\boldsymbol{r})\, w(s,\boldsymbol{r})\Big) + \nabla q(s,\boldsymbol{r})\cdot\nabla\lambda(1-s,\boldsymbol{r})\Big)\delta\phi(\boldsymbol{r})\, ds\, d\Gamma$$
$$-\int_{\Gamma\times T} \kappa(\boldsymbol{r})\lambda(1-s,\boldsymbol{r})\alpha(s)q(s,\boldsymbol{r})\delta\phi(\boldsymbol{r})\, d\Gamma\, ds$$
$$-\int_{\Gamma\times T} \alpha(s)\partial_{\boldsymbol{n}}(\lambda(1-s,\boldsymbol{r})q(s,\boldsymbol{r}))\delta\phi(\boldsymbol{r})\, d\Gamma\, ds$$

and inserting $-q^\dagger$ instead of λ:

$$\delta L_{\delta\phi} = -\int_{\Gamma\times T} q(s,\boldsymbol{r})\delta(s=1)\delta\phi\, ds\, d\Gamma$$
$$+\int_{\Gamma\times T} \Big(q^\dagger(1-s,\boldsymbol{r})\Big(q_s(s,\boldsymbol{r}) + q(s,\boldsymbol{r})\, w(s,\boldsymbol{r})\Big) + \nabla q(s,\boldsymbol{r})\cdot\nabla q^\dagger(1-s,\boldsymbol{r})\Big)\delta\phi(\boldsymbol{r})\, ds\, d\Gamma \tag{11}$$
$$+\int_{\Gamma\times T} \alpha(s)(\kappa(\boldsymbol{r}) + \partial_{\boldsymbol{n}})(q^\dagger(1-s,\boldsymbol{r})q(s,\boldsymbol{r}))\delta\phi(\boldsymbol{r})\, d\Gamma\, ds.$$

One can see that in the case of a Neumann boundary condition the last two terms drop out and that we recover the expression given by equation (12):

$$\delta L_{\delta\phi} = -\int_{\Gamma\times T} q\delta(s=1)\delta\phi(\boldsymbol{r})\, ds\, d\Gamma$$
$$+\int_{\Gamma\times T} q^\dagger(1-s,\boldsymbol{r})\Big(q_s(s,\boldsymbol{r}) + q(s,\boldsymbol{r})w(\boldsymbol{r})\Big)\delta\phi(\boldsymbol{r})\, ds\, d\Gamma \tag{12}$$
$$+\int_{\Gamma\times T} \nabla q(s,\boldsymbol{r})\cdot\nabla q^\dagger(1-s,\boldsymbol{r})\delta\phi(\boldsymbol{r})\, ds\, d\Gamma.$$

Likewise, in the case of a Dirichlet boundary condition the two last terms drop out and using integration by parts on Γ in equation (11) along with the p.d.e. for q, one recovers equation (13):

$$\delta L \cdot \delta\phi = -\int_{\Gamma\times T} \Big(q(s,\boldsymbol{r})\delta(s=1) + \frac{\partial q^\dagger(1-s,\boldsymbol{r})}{\partial \boldsymbol{n}}\frac{\partial q(s,\boldsymbol{r})}{\partial \boldsymbol{n}}\Big)\delta\phi(\boldsymbol{r})\, d\Gamma\, ds. \tag{13}$$

To provide the derivation in a level set framework we first proceed as follows:

$$\delta Q_{\delta\phi} = -\frac{1}{V}\int_{\Gamma} q(s=1,\boldsymbol{r})\delta\phi(\boldsymbol{r}) + \frac{1}{V}\int_{\Omega}\delta q(s=1,\boldsymbol{r})\, d\boldsymbol{r}. \tag{14}$$

We now define $\delta Q_{stress} = \frac{1}{V}\int_\Omega \delta q(s=1,\boldsymbol{r})\, d\boldsymbol{r}$ and deriving δQ_{stress} with respect to $\delta\phi(\boldsymbol{y})$, we obtain:

$$\frac{\delta Q_{stress}}{\delta\phi(\boldsymbol{y})} = \frac{1}{V}\int_{\Omega}\frac{\delta q(s=1,\boldsymbol{r})}{\delta\phi(\boldsymbol{y})}\, d\boldsymbol{r}. \tag{15}$$

Define $g(s,\boldsymbol{r},\boldsymbol{y}) = \frac{\delta q(s,\boldsymbol{r})}{\delta\phi(\boldsymbol{y})}$ with $g(s=0)=0$ as initial condition. We write a PDE for g when w is kept constant but we move the domain:

$$\frac{\delta q_s(s,\boldsymbol{r},\boldsymbol{y})}{\delta\phi(\boldsymbol{y})} = \frac{\delta\Delta q(s,\boldsymbol{r},\boldsymbol{y})}{\delta\phi(\boldsymbol{y})} - \frac{\delta q(s,\boldsymbol{r},\boldsymbol{y})}{\delta\phi(\boldsymbol{y})}w(s,\boldsymbol{r}) - \frac{\delta w(s,\boldsymbol{r})}{\delta\phi(\boldsymbol{y})}q(s,\boldsymbol{r},\boldsymbol{y}). \tag{16}$$

Interchanging δ with the s derivative and the laplacian and using that w is kept constant the following PDE is obtained for g:

$$g_s(s,\boldsymbol{r},\boldsymbol{y}) = \Delta g(s,\boldsymbol{r},\boldsymbol{y}) - g(s,\boldsymbol{r},\boldsymbol{y})w(s,\boldsymbol{r}) \tag{17}$$

$$\begin{aligned}
\frac{\delta Q_{stress}(s)}{\delta\phi(\boldsymbol{y})} =& \\
&\frac{1}{V}\int_{\Omega} g(s,\boldsymbol{r},\boldsymbol{y})d\boldsymbol{r} = \\
&\frac{1}{V}\int_{\Omega} \underbrace{q^\dagger(s=0,\boldsymbol{r})}_{=1} g(s,\boldsymbol{r},\boldsymbol{y}) - \underbrace{g(s=0,\boldsymbol{r},\boldsymbol{y})}_{=0} q^\dagger(s,\boldsymbol{r})d\boldsymbol{r} = \\
&\frac{1}{V}\int_{\Omega\times T} (q^\dagger(s-t,\boldsymbol{r})g(t,\boldsymbol{r},\boldsymbol{y}))_t dt d\boldsymbol{r} = \\
&\frac{1}{V}\int_{\Omega\times T} g_t(t,\boldsymbol{r},\boldsymbol{y})q^\dagger(s-t,\boldsymbol{r}) - g(t,\boldsymbol{r},\boldsymbol{y})q^\dagger_t(s-t,\boldsymbol{r})dtd\boldsymbol{r} = \\
&\frac{1}{V}\int_{\Omega\times T} (\Delta g(t,\boldsymbol{r},\boldsymbol{y}) - g(t,\boldsymbol{r},\boldsymbol{y})\, w(\boldsymbol{r}))q^\dagger(s-t,\boldsymbol{r}) - g(s,\boldsymbol{r},\boldsymbol{y})(\Delta q^\dagger(s-t,\boldsymbol{r}) - q^\dagger(s-t,\boldsymbol{r})\, w(\boldsymbol{r}))dtd\boldsymbol{r} = \\
&\frac{1}{V}\int_{\Omega\times T} \Delta g(t,\boldsymbol{r},\boldsymbol{y})q^\dagger(s-t,\boldsymbol{r}) - g(t,\boldsymbol{r},\boldsymbol{y})\Delta q^\dagger(s-t,\boldsymbol{r})d\sigma d\boldsymbol{r} = \\
&\frac{1}{V}\int_{\Gamma\times T} \underbrace{q^\dagger(s-t,\boldsymbol{r})}_{=0 \text{ for Dirichlet}} \nabla g(t,\boldsymbol{r},\boldsymbol{y})\cdot\nabla\phi(\boldsymbol{r}) - g(t,\boldsymbol{r},\boldsymbol{y})\underbrace{\nabla q^\dagger(s-t,\boldsymbol{r})\cdot\nabla\phi(\boldsymbol{r})}_{=0 \text{ for Neumann}} dtd\Gamma,
\end{aligned} \tag{18}$$

where $\boldsymbol{n} = \frac{\nabla\phi(\boldsymbol{r})}{|\nabla\phi(\boldsymbol{r})|}$ and we assume $\phi(\boldsymbol{r})$ is a signed distance function, i.e. $|\nabla\phi(\boldsymbol{r})| = 1$. In the case of Dirichlet boundary conditions $q(s,\boldsymbol{r}_\Gamma(\phi),\phi) = 0$, where $\boldsymbol{r}_\Gamma$ describes the position of the interface Γ, and take the derivative with respect to $\delta\phi(\boldsymbol{y})$:

$$\frac{\delta q(s,\boldsymbol{r}_\Gamma(\phi),\phi)}{\delta\phi(\boldsymbol{y})} + \nabla q(s,\boldsymbol{r}_\Gamma(\phi),\phi)\cdot\frac{\delta\boldsymbol{r}_\Gamma}{\delta\phi(\boldsymbol{y})} = 0. \tag{19}$$

Inserting the Dirichlet boundary conditions in (18), i.e. $q^\dagger(\boldsymbol{r}, s-t)=0$, and using $\frac{\delta \boldsymbol{r}_\Gamma(\boldsymbol{\phi})}{\delta\phi(\boldsymbol{y})} = -\nabla\phi(\boldsymbol{r})\delta(\boldsymbol{r}_\Gamma - \boldsymbol{y})$ for a reinitialized $\phi(\boldsymbol{r})$ we obtain:

$$\delta Q_{stress}(s) = \frac{1}{V}\int\limits_{\Gamma\times T} -\frac{\partial q(t,\boldsymbol{r})}{\partial \boldsymbol{n}}\frac{\partial q^\dagger(s-t,\boldsymbol{r})}{\partial \boldsymbol{n}}\delta\phi(\boldsymbol{r})dtd\boldsymbol{r}. \tag{20}$$

We note the equivalence between equation (13) and equation (20).

In the case of Neumann we write the Neumann boundary conditions as $f(\boldsymbol{r}_\Gamma(\phi),\phi) = \nabla q(\boldsymbol{r}_\Gamma)\cdot\nabla\phi(\boldsymbol{r}) = 0$:

$$\frac{\delta f(\boldsymbol{r}_\Gamma(\phi),\phi)}{\delta\phi(\boldsymbol{y})} = \frac{\delta\nabla q(\boldsymbol{r}_\Gamma)}{\delta\phi(\boldsymbol{y})}\cdot\nabla\phi(\boldsymbol{r}_\Gamma)\delta\phi(\boldsymbol{r}_\Gamma) + \nabla q(\boldsymbol{r}_\Gamma)\frac{\delta\nabla\phi(\boldsymbol{r}_\Gamma)}{\delta\phi(\boldsymbol{y})} + \nabla(\nabla q\cdot\nabla\phi(\boldsymbol{r}_\Gamma))\frac{\delta\boldsymbol{r}_\Gamma}{\delta\phi(\boldsymbol{y})}. \tag{21}$$

Inserting the boundary conditions as in the Dirichlet case into (18) we get:

$$\delta Q_{stress}(s) = \frac{1}{V}\int\limits_{\Gamma\times T} q^\dagger(s-t,\boldsymbol{r})\left(\frac{\partial^2 q(t,\boldsymbol{r})}{\partial \boldsymbol{n}^2}\delta\phi(\boldsymbol{r}) - \nabla q(t,\boldsymbol{r})\cdot\nabla\delta\phi(\boldsymbol{r})\right)dtd\boldsymbol{r}. \tag{22}$$

Now, using integrating by parts on the surface Γ it can be decomposed into terms of $\delta\phi$ and terms of $\nabla\delta\phi$:

$$\begin{aligned}
&\int\limits_{\Gamma\times T} q^\dagger(1-s,\boldsymbol{r})\left(\frac{\partial^2 q(s,\boldsymbol{r})}{\partial \boldsymbol{n}^2}\delta\phi(\boldsymbol{r}) - \nabla q(s,\boldsymbol{r})\cdot\nabla\delta\phi(\boldsymbol{r})\right)d\Gamma ds \\
&= \int\limits_{\Gamma\times T} q^\dagger(1-s,\boldsymbol{r})\Delta q(s,\boldsymbol{r})\delta\phi(\boldsymbol{r}) + \nabla q(s,\boldsymbol{r})\cdot\nabla q^\dagger(1-s,\boldsymbol{r})\delta\phi(\boldsymbol{r}) \\
&- \frac{\partial q(s,\boldsymbol{r})}{\partial \boldsymbol{n}}\frac{\partial q^\dagger(1-s,\boldsymbol{r})\delta\phi(\boldsymbol{r})}{\partial \boldsymbol{n}} - \kappa q^\dagger(1-s,\boldsymbol{r})\delta\phi(\boldsymbol{r})\frac{\partial q(s,\boldsymbol{r})}{\partial \boldsymbol{n}}\,d\Gamma\,ds \\
&= \int\limits_{\Gamma\times T} q^\dagger(1-s,\boldsymbol{r})\Delta q(s,\boldsymbol{r})\delta\phi(\boldsymbol{r}) + \nabla q(s,\boldsymbol{r})\cdot\nabla q^\dagger(1-s,\boldsymbol{r})\delta\phi(\boldsymbol{r})\,d\Gamma\,ds \\
&= \int\limits_{\Gamma\times T} \Big(q^\dagger(1-s,\boldsymbol{r})\big[q_s(s,\boldsymbol{r}) + q(s,\boldsymbol{r})w(\boldsymbol{r})\big] + \nabla q(s,\boldsymbol{r})\cdot\nabla q^\dagger(1-s,\boldsymbol{r})\Big)\delta\phi(\boldsymbol{r})\,d\Gamma\,ds,
\end{aligned} \tag{23}$$

where in the first equality we use integration by parts on the surface, in the second equality we use the fact that $\frac{\partial q}{\partial \boldsymbol{n}} = 0$ and $\frac{\partial(q^\dagger\delta\phi)}{\partial \boldsymbol{n}} = 0$ and in the third we use the PDE. Again we note the equivalence between equation (12) and equation (22).

In the case of Robin boundary conditions, $f(\boldsymbol{r}_\Gamma(\phi),\phi) = \nabla q(\boldsymbol{r}_\Gamma)\cdot\nabla\phi(\boldsymbol{r}) + \alpha(s)q(\boldsymbol{r}_\Gamma) = 0$:

$$\begin{aligned}
&\frac{\delta f(\boldsymbol{r}_\Gamma(\phi),\phi)}{\delta\phi(\boldsymbol{y})} = \\
&\frac{\delta\nabla q(\boldsymbol{r}_\Gamma)}{\delta\phi(\boldsymbol{y})}\cdot\nabla\phi(\boldsymbol{r}_\Gamma)\delta\phi(\boldsymbol{r}_\Gamma) + \nabla q(\boldsymbol{r}_\Gamma)\frac{\delta\nabla\phi(\boldsymbol{r}_\Gamma)}{\delta\phi(\boldsymbol{y})} + \nabla(\nabla q\cdot\nabla\phi(\boldsymbol{r}_\Gamma))\frac{\delta\boldsymbol{r}_\Gamma}{\delta\phi(\boldsymbol{y})} + \\
&\alpha(s)\left(\frac{\delta q(s,\boldsymbol{r}_\Gamma(\phi),\phi)}{\delta\phi(\boldsymbol{y})} + \nabla q(s,\boldsymbol{r}_\Gamma(\phi),\phi)\cdot\frac{\delta\boldsymbol{r}_\Gamma}{\delta\phi(\boldsymbol{y})}\right).
\end{aligned} \tag{24}$$

Inserting the boundary conditions as in the Dirichlet and Neumann cases into (18) and transforming $\frac{\partial q^\dagger(s-t,\boldsymbol{r})}{\partial \boldsymbol{n}}$ to $-\alpha^\dagger(s-t)q^\dagger(s-t,\boldsymbol{r})$ we get:

$$\delta Q_{stress}(s) = \frac{1}{V}\int\limits_{\Gamma\times T} q^\dagger(s-t,\boldsymbol{r})\left(\frac{\partial^2 q(t,\boldsymbol{r})}{\partial \boldsymbol{n}^2} + \alpha(t)\frac{\partial q(t,\boldsymbol{r})}{\partial \boldsymbol{n}}\right)\delta\phi(\boldsymbol{r}) - \nabla q(t,\boldsymbol{r})\cdot\nabla\delta\phi(\boldsymbol{r})\,dtd\boldsymbol{r}. \tag{25}$$

Now, using integrating by parts on the surface Γ it can be decomposed into terms of $\delta\phi$ and terms of $\nabla\delta\phi$:

$$\begin{aligned}
&\int_{\Gamma\times T} q^\dagger(1-s,\boldsymbol{r})\left(\frac{\partial^2 q(s,\boldsymbol{r})}{\partial \boldsymbol{n}^2}+\alpha(s)\frac{\partial q(s,\boldsymbol{r})}{\partial \boldsymbol{n}}\right)\delta\phi(\boldsymbol{r})-\nabla q(s,\boldsymbol{r})\cdot\nabla\delta\phi(\boldsymbol{r}))\,d\Gamma ds\\
&\quad=\int_{\Gamma\times T} q^\dagger(1-s,\boldsymbol{r})\Delta q(s,\boldsymbol{r})\delta\phi(\boldsymbol{r})+\nabla q(s,\boldsymbol{r})\cdot\nabla q^\dagger(1-s,\boldsymbol{r})\delta\phi(\boldsymbol{r})\\
&\quad-\frac{\partial q(s,\boldsymbol{r})}{\partial \boldsymbol{n}}\frac{\partial q^\dagger(1-s,\boldsymbol{r})\delta\phi(\boldsymbol{r})}{\partial \boldsymbol{n}}-\kappa q^\dagger(1-s,\boldsymbol{r})\delta\phi(\boldsymbol{r})\frac{\partial q(s,\boldsymbol{r})}{\partial \boldsymbol{n}}\,d\Gamma\,ds\\
&\quad+\int_{\Gamma\times T}\alpha(s)q^\dagger(1-s,\boldsymbol{r})\frac{\partial q(s,\boldsymbol{r})}{\partial \boldsymbol{n}}\delta\phi(\boldsymbol{r})\,d\Gamma\,ds\\
&\quad=\int_{\Gamma\times T} q^\dagger(1-s,\boldsymbol{r})\Delta q(s,\boldsymbol{r})\delta\phi(\boldsymbol{r})+\nabla q(s,\boldsymbol{r})\cdot\nabla q^\dagger(1-s,\boldsymbol{r})\delta\phi(\boldsymbol{r})\\
&\quad+\alpha(s)(\kappa(\boldsymbol{r})+\partial_{\boldsymbol{n}})(q(s,\boldsymbol{r})q^\dagger(1-s,\boldsymbol{r}))\delta\phi(\boldsymbol{r})\,d\Gamma\,ds\\
&\quad=\int_{\Gamma\times T}\Big(q^\dagger(1-s,\boldsymbol{r})\big[q_s(s,\boldsymbol{r})+q(s,\boldsymbol{r})w(\boldsymbol{r})\big]+\nabla q(s,\boldsymbol{r})\cdot\nabla q^\dagger(1-s,\boldsymbol{r})\Big)\delta\phi(\boldsymbol{r})\,d\Gamma\,ds,\\
&\quad+\int_{\Gamma\times T}\alpha(s)(\kappa(\boldsymbol{r})+\partial_{\boldsymbol{n}})(q(s,\boldsymbol{r})q^\dagger(1-s,\boldsymbol{r}))\delta\phi(\boldsymbol{r})\,d\Gamma\,ds,
\end{aligned}$$

where in the first equality we use integration by parts on the surface, in the second equality we use the fact that $\frac{\partial q}{\partial \boldsymbol{n}}=-\alpha(s)q$ and $\frac{\partial\delta\phi}{\partial \boldsymbol{n}}=0$ and in the third we use the PDE. Again we note the equivalence of this expression with equation (11). We have performed tests (not presented here) using the finite difference approximation to the shape derivative to guarantee it converges to the analytical result in the cases of the different boundary conditions we consider, i.e. Dirichlet, Neumann and Robin.

3.4. Remarks

1. In the case of homogeneous Neumann boundary conditions, we have $\nabla q\cdot\nabla q^\dagger=\frac{\partial q}{\partial\boldsymbol{\tau}}\frac{\partial q^\dagger}{\partial\boldsymbol{\tau}}$, where $\boldsymbol{\tau}$ is the tangential vector to the boundary Γ.
2. We can use the factorization property of the partition function to write a more transparent expression for the shape derivative: $Q=\frac{1}{V}\int_\Omega q(\boldsymbol{r},s)q^\dagger(\boldsymbol{r},1-s)\,d\boldsymbol{r}$ for any s. Thus choosing $s=1$ gives $Q=\frac{1}{V}\int_\Omega q(\boldsymbol{r},s=1)\underbrace{q^\dagger(\boldsymbol{r},s=0)}_{=1}\,d\boldsymbol{r}$ and choosing $s=0$ gives $Q=\frac{1}{V}\int_\Omega\underbrace{q(\boldsymbol{r},s=0)}_{=1}q^\dagger(\boldsymbol{r},s=1)\,d\boldsymbol{r}$. Thus one can write $Q=\frac{1}{2V}\int_\Omega q(\boldsymbol{r},s=1)+q^\dagger(\boldsymbol{r},s=1)\,d\boldsymbol{r}$, and by interchanging q and $q^\dagger$ in equation (12) (or (22)), one can write the following:

$$\begin{aligned}
\delta L_{\delta\phi}&=-\int_{\Gamma\times T} q\delta(s=1)\delta\phi(\boldsymbol{r})\,ds\,d\Gamma\\
&+\int_{\Gamma\times T} q^\dagger(1-s,\boldsymbol{r})\big[q_s(s,\boldsymbol{r})+q(s,\boldsymbol{r})w(\boldsymbol{r})\big]\delta\phi(\boldsymbol{r})\,ds\,d\Gamma\\
&+\int_{\Gamma\times T}\nabla q(s,\boldsymbol{r})\cdot\nabla q^\dagger(1-s,\boldsymbol{r})\delta\phi(\boldsymbol{r})\,ds\,d\Gamma\\
&=\int_{\Gamma\times T}\Big(-q(s,\boldsymbol{r})\delta(s=1)+q^\dagger(1-s,\boldsymbol{r})\Delta q(s,\boldsymbol{r})+\nabla q(s,\boldsymbol{r})\cdot\nabla q^\dagger(1-s,\boldsymbol{r})\Big)\delta\phi(\boldsymbol{r})\,ds\,d\Gamma
\end{aligned}\tag{26}$$

$$= \int_{\Gamma\times T} \Big(-\frac{1}{2}\Big[q(s,\boldsymbol{r})\delta(s=1) + q^\dagger(1-s,\boldsymbol{r})\delta(s=0)\Big] + \frac{1}{2}q^\dagger(1-s,\boldsymbol{r})\Delta q(s,\boldsymbol{r}) + \frac{1}{2}q(s,\boldsymbol{r})\Delta q^\dagger(1-s,\boldsymbol{r})$$
$$+ \nabla q(s,\boldsymbol{r})\cdot\nabla q^\dagger(1-s,\boldsymbol{r})\Big)\delta\phi(\boldsymbol{r})\, ds\, d\Gamma$$
$$= \frac{1}{2}\int_{\Gamma\times T} \Big(-\Big[q(s,\boldsymbol{r})\delta(s=1) - q^\dagger(1-s,\boldsymbol{r})\delta(s=0)\Big] + \Delta\Big[q(s,\boldsymbol{r})q^\dagger(1-s,\boldsymbol{r})\Big]\Big)\delta\phi(\boldsymbol{r})\, ds\, d\Gamma.$$

Using equation (4) we obtain the following symmetric expression:

$$\delta L_{\delta\phi} = -\frac{1}{2}\int_\Gamma \Big(q(1,\boldsymbol{r}) + q^\dagger(1,\boldsymbol{r}) - Q\,\Delta f_+(\boldsymbol{r})\Big)\delta\phi(\boldsymbol{r})\, d\Gamma, \tag{27}$$

and when we evolve the SCFT fields with equations (4) and can assume $f_+(\boldsymbol{r}) \approx 0$

$$\delta L_{\delta\phi} = -\frac{1}{2}\int_\Gamma \Big(q(1,\boldsymbol{r}) + q^\dagger(1,\boldsymbol{r})\Big)\delta\phi(\boldsymbol{r})\, d\Gamma. \tag{28}$$

3. For Robin boundary conditions we can obtain a symmetric expression as in Neumann for the first terms, and by inserting the densities ρ_A, ρ_B instead of $q, q^\dagger$ in the second integral of (11) and make use of the boundary conditions to obtain:

$$\delta Q_{stress} = \frac{1}{2}\int_\Gamma \Big(Q\,\Delta f_+(\boldsymbol{r}) - (\kappa(\boldsymbol{r}) + \partial_{\boldsymbol{n}})(\alpha_A\rho_A(\boldsymbol{r}) + \alpha_B\rho_B(\boldsymbol{r}))\Big)\delta\phi(\boldsymbol{r})\, d\Gamma. \tag{29}$$

In addition if we use that $\alpha_A\rho_A + \alpha_B\rho_B = -\partial_{\boldsymbol{n}}(\rho_A + \rho_B)$ the last term can be written as $(\kappa(\boldsymbol{r})\partial_{\boldsymbol{n}} + \partial_{\boldsymbol{n}n})(-Q f_+(\boldsymbol{r}))$, and get the following symmetric expression:

$$\delta Q_{stress} = \frac{1}{2}\int_\Gamma Q\,(\Delta + \kappa(\boldsymbol{r})\partial_{\boldsymbol{n}} + \partial_{\boldsymbol{n}n}) f_+(\boldsymbol{r})\delta\phi(\boldsymbol{r})\, d\Gamma. \tag{30}$$

4. Shape optimization algorithm using the level-set derivatives and examples

In the case of free surface polymers, the self-assembly process is described by the saddle point of the Hamiltonian, H, with respect to the fields $w_-(\boldsymbol{r})$ and $w_+(\boldsymbol{r})$ as well as with respect to the shape, here encoded by the level-set function $\phi(\boldsymbol{r})$. In this section, we provide a few examples to illustrate potential applications of the shape derivatives derived in this manuscript. In particular, we are focusing on illustrating that the energy of the systems considered decreases in the case where the domain's boundary is taken as one of the free parameters of the optimization process. These examples show how a polymeric material with a free surface will change its shape in order to decrease its energy and transit to a locally stable state with a lower energy. The examples in two spatial dimensions could be useful in the context of directed self-assembly and the positioning of channels in integrated circuits or in the study of self-assembly in free surface droplets; the example in three spatial dimensions could be relevant to the study of free surface polymeric melts such as cubosomes [36,35,37,10,14,26,22].

Algorithm 1 describes the numerical steps we use to minimize $H[w_-(\boldsymbol{r}), w_+(\boldsymbol{r}), \phi(\boldsymbol{r})]$. The optimization with respect to the fields is obtained by solving the standard SCFT equations of section 2 (see Algorithm 2). In our work, we use the framework introduced in Ouaknin et al. [31,30] which imposes a Neumann boundary condition for q, as first proposed in [7], using the method of Papac et al. [33,34]. We encoded the numerical solution of the Fokker–Planck equations and the level set equations in quad/oct trees as described in [24,23] and their parallelization on adaptive grids as in Mirzadeh et al. [25]. The optimization with respect to the shape drives the boundary Γ to a local saddle point. In our work, the boundary motion is described by the level-set equation:

$$\frac{\partial\phi(\boldsymbol{r})}{\partial t} + v_n(\boldsymbol{r})|\nabla\phi(\boldsymbol{r})| = 0, \tag{31}$$

where $v_n(\boldsymbol{r})$ is the normal velocity at Γ. We use the functional level-set derivatives derived in section 3 and choose $\delta\phi(\boldsymbol{r}) = -\dfrac{\delta H}{\delta\phi(\boldsymbol{r})}$ so that the total variation of the free energy is decreased: $\delta H = -\displaystyle\int_\Gamma \left|\frac{\delta H}{\delta\phi(\boldsymbol{r})}\right|^2 d\Gamma < 0$. We thus define $v_n(\boldsymbol{r})$ to be

Algorithm 1 Procedure to find the saddle point of H with optimal shape.

I. Perform Algorithm 2
II.
while $||\delta H/\delta\phi||_2 > \epsilon_\phi$ **do** // ϵ_ϕ is a chosen tolerance.
1. Perform 1–4 steps of Algorithm 2
2. Find the velocity for $\phi(\boldsymbol{r})$ and advect $\phi(\boldsymbol{r})$ every $O(100)$ mean-field steps
3. $t = t + 1$
III. Perform Algorithm 2

Algorithm 2 Procedure to find the saddle point of H with respect to the fields w_- and w_+ (SCFT).

while $||\delta H/\delta\omega||_2 > \epsilon_w$ **do** // ϵ_w is a chosen tolerance.
1. Solve two Fokker Planck equations $q(s,\boldsymbol{r}), q^\dagger(s,\boldsymbol{r})$
2. compute the densities $\rho_A(\boldsymbol{r}), \rho_B(\boldsymbol{r})$
3. compute the force for $w_+(\boldsymbol{r})$ and $w_-(\boldsymbol{r})$
4. advance the potentials $w_-(\boldsymbol{r}), w_+(\boldsymbol{r})$
5. $t = t + 1$

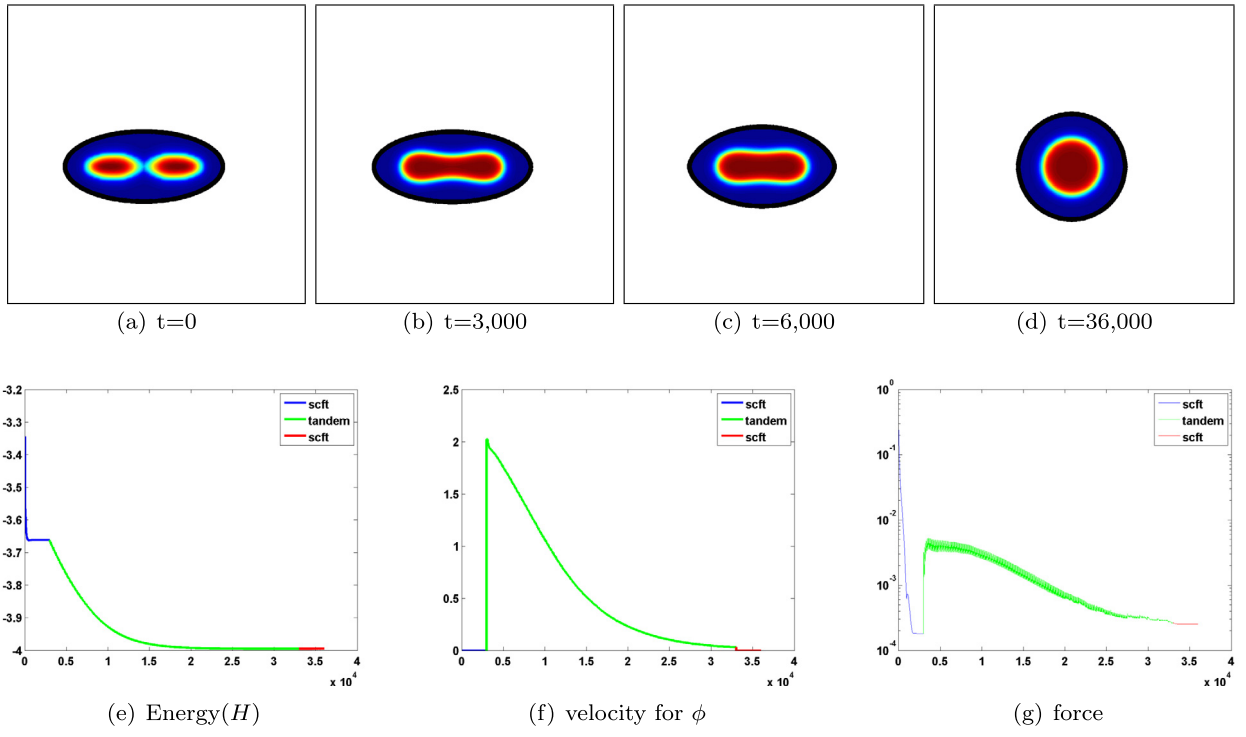

(a) t=0 (b) t=3,000 (c) t=6,000 (d) t=36,000

(e) Energy(H) (f) velocity for ϕ (g) force

Fig. 3. Evolution of the densities and the shape: starting from a free surface with elliptical shape and a minority region enclosed into two ellipses, both the boundary and the minority region transit to a disk shape. One can also observe a change in topology in the minority region. The change in shape leads to an energy drop of $\Delta H_{\Delta\phi} = -0.334$. The shape is advected in the tandem phase (green) where the SCFT force oscillates during this phase. The parameters for this simulation are $(f_A, \chi_{AB}) = (0.3, 36)$, $L_x = 12.8R_g$, $\gamma = 0$ and $\Delta s = 0.01$. (For interpretation of the references to color in this figure legend, the reader is referred to the web version of this article.)

proportional to $\dfrac{\delta H}{\delta\phi(\boldsymbol{r})}$ as in equation (6). Specifically, the velocity is computed inside Ω and is extrapolated in a narrow band outside the domain by solving:

$$\frac{\partial v_n(\boldsymbol{r})}{\partial\xi} + \mathcal{H}\Big(\phi(\boldsymbol{r})\Big)\nabla v_n(\boldsymbol{r}) \cdot \nabla\phi(\boldsymbol{r}) = 0, \tag{32}$$

in order to have a well-defined normal velocity at the vicinity of the zero level set of ϕ, where ξ is a pseudo-time variable. A similar equation is also used to extrapolate the statistical fields w_+ and w_-, which are needed to compute the Fokker–Planck equation in the advected domain $\phi^{\tau+1}(\boldsymbol{r}) < 0$. Finally the level-set function is transformed into a signed distance function [27,38,23]:

$$\frac{\partial\phi(\boldsymbol{r})}{\partial\xi} + \text{signum}\Big(\phi(\boldsymbol{r})\Big)\Big(|\nabla\phi(\boldsymbol{r})| - 1\Big) = 0, \tag{33}$$

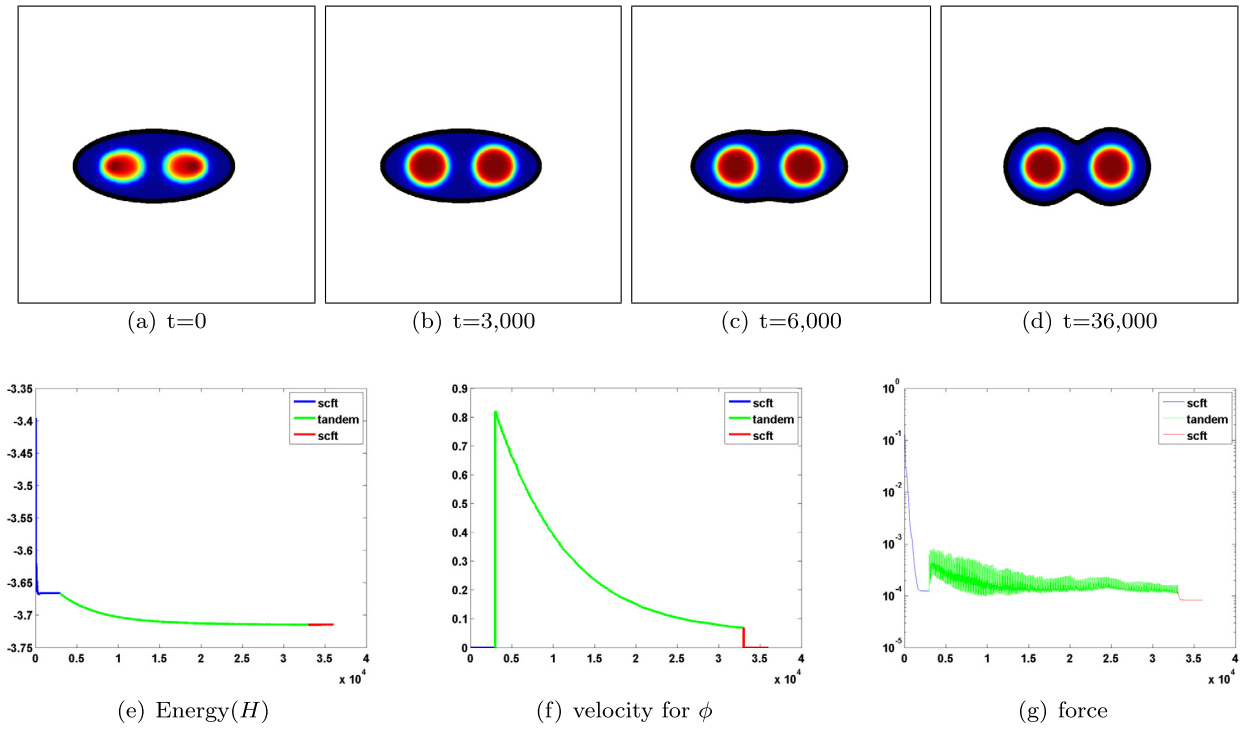

Fig. 4. Same example as in Fig. 3, but this time the seeded minority components are located farther apart. Here, the energy drop is $\Delta H_{\Delta\phi} = -0.0487$. The shape is advected in the tandem phase (green) where the SCFT force oscillates during this phase. The parameters for this simulation are $(f_A, \chi_{AB}) = (0.3, 36)$, $L_x = 12.8R_g$, $\gamma = 0$ and $\Delta s = 0.01$. (For interpretation of the references to color in this figure legend, the reader is referred to the web version of this article.)

which is desired for the numerical algorithms used in this paper. For all the level set equations we use a Gudonov scheme on adaptive trees as described in Min and Gibou [23]. To regularize the shape, we add to the normal velocity a surface tension term $\gamma\kappa$, where $\gamma > 0$ is a chosen parameter, and we discretize this term as in [28]. In all of the examples presented below, the volume and the amount of material are kept constant by subtracting the average velocity from the velocity obtained by computing the shape derivative.

In all of the examples, we first only evolve the fields for $O(1000)$ mean-field steps until we reach a local saddle point. Then we evolve the fields for another $O(10,000)$ mean-field steps, but this time in tandem with the optimization with respect to ϕ, which we evolve every $O(100)$ mean-field steps. Finally, we fix the boundary and relax the fields for another $O(1000)$ mean-field steps until we reach a new saddle point. This procedure ensures that, by changing the shape, we decrease the energy. Figs. 3(e), 4(e), 5(e) and 6(e) depicts the decrease in energy during each of the three steps, confirming that the shape derivatives we developed can be used to optimize the coupled fields and shape in both two and three spatial dimensions.

Figs. 3(f), 4(f), 5(f) and 6(f) illustrate the decrease in the norm of the shape gradient, i.e. the velocity $||\boldsymbol{v}||_2$ for updating ϕ during the shape optimization phase. As described in Algorithm 1, the shape is fixed during the first and last phases. During the intermediate phase, which we call the 'tandem' phase, the shape is evolved every $O(100)$ mean field steps until $||\boldsymbol{v}||_2$ is smaller than a chosen tolerance ϵ_ϕ.

Figs. 3(g), 4(g), 5(g) and 6(g) depict the evolution of the SCFT force $(\max(||f_+||_2, ||f_-||_2))$ during the three phases of the mixed SCFT-shape optimization process. In the 'tandem' phase, we note that the SCFT force increases after each shape advection step because the statistical fields need to adjust to the incremental change in shape. As described in Algorithm 2, the shape is fixed in the first and last phase while the statistical fields are updated until the energy reaches a steady-state value. We define $\Delta H_{\Delta\phi}$ as the difference of energy of the polymer between its initial shape and its optimized shape, which corresponds to the end of phase I and the end of phase III of Algorithm 1, respectively.

As it is always the case in optimization problems that may have multiple local optimal points, the initial data (here the seed in the fields, which in turn define the polymer densities) influences which local saddle point (or metastable equilibrium) is reached. Figs. 3 and 4 present the results of the shape optimization process obtained with two different seeds, which lead to significant differences in both the topology of the densities as well as in the shape of the free boundary.

Fig. 5 provides an example where the seed consists of a random distribution in the statistical fields inside a circular free boundary. The optimization process leads to a symmetric density morphology. Interestingly, the minority region wets the free surface and locally changes the curvature in order to reduce the AB interfacial region.

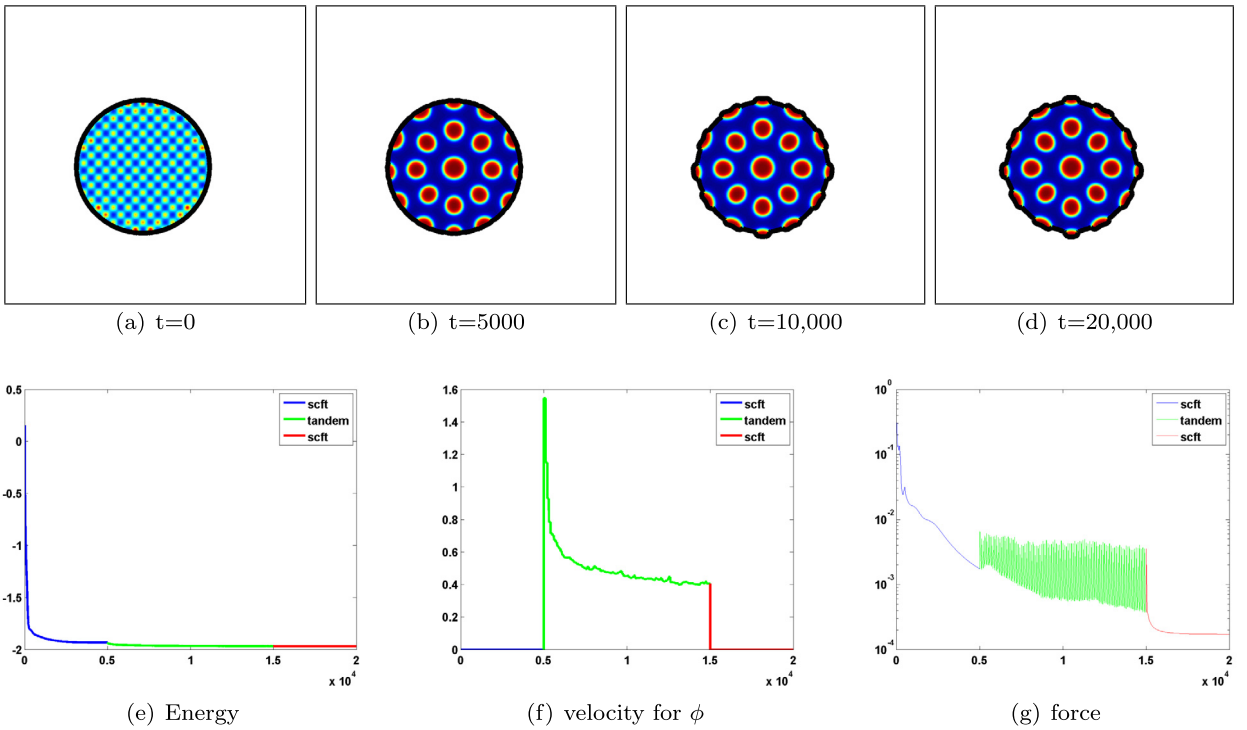

Fig. 5. Evolution of the densities and the free boundary: starting from a random density distribution enclosed by a circular free surface, the minority region self-assembles into a circular morphology. The energy decreases by $\Delta H_{\Delta\phi} = -0.0357$. The shape is advected in the tandem phase (green) where the SCFT force oscillates during this phase. The parameters for this simulation are $(f_A, \chi_{AB}) = (0.3, 25)$, $\gamma = 0.5/R_g$ and $\Delta s = 0.005$. (For interpretation of the references to color in this figure legend, the reader is referred to the web version of this article.)

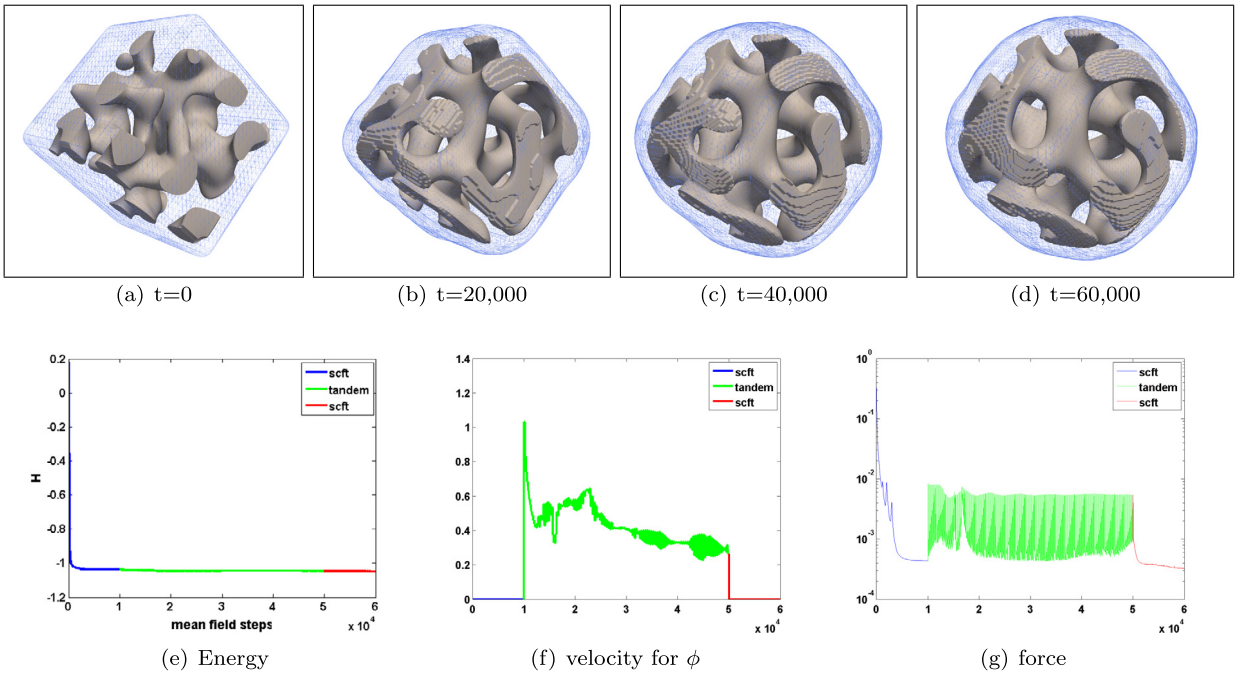

Fig. 6. Evolution of the density and the shape: starting with a cube for the shape and a gyroid seed for the A component. The energy drop is $\Delta H_{\Delta\phi} = -0.0115$. The shape is advected in the tandem phase (green) where the SCFT force oscillates during this phase. The parameters are $(f_A, \chi_{AB}) = (0.36, 20)$, $\gamma = 1.00/R_g$, $L_x = 18R_g$, and $\Delta s = 0.005$. (For interpretation of the references to color in this figure legend, the reader is referred to the web version of this article.)

Fig. 6 provides an numerical example in three spatial dimensions that is motivated by the study of cubosomes, which are cubic bicontinuous network morphologies that have gained a lot of attention recently particularly because of their potential in food sciences and as drug delivery carriers [14,26,22]. Starting with a gyroid seed for the minority density enclosed into a cubic free surface, the self-assembly process drives the morphology of both the minority density and the free surface to a nontrivial geometry. In this case, the energy drop is $\Delta H_{\Delta\phi} = -0.0115$, illustrating that complex three dimensional configurations can be treated by our formalism.

5. Conclusion

We derived functional level-set derivatives for the cases of homogeneous Dirichlet, Neumann and Robin boundary conditions in the context of polymer self-consistent field theory. Using these shape derivatives in the Neumann case, we provided numerical examples of free boundary SCFT simulations for diblock copolymer melts in two and three spatial dimensions. The minimization process takes into account the shape of the free boundary in addition to the statistical fields, which can enable studies of their coupling. In all the cases studied, the minimization leads to locally stable states with decreased energy. This work could be used for the exploration of the free surface assembly of a wide range of polymeric materials.

Acknowledgements

This research was supported in part by ARO W911NF-16-1-0136 and the NSF under the DMS 1620471. KD and GHF acknowledge support from the NSF under the DMREF program DMR-1332842. This work used the Extreme Science and Engineering Discovery Environment (XSEDE), which is supported by National Science Foundation grant number ACI-1053575. The authors acknowledge the Texas Advanced Computing Center (TACC) at The University of Texas at Austin as well as the San Diego supercomputing center at UCSD for providing HPC and visualization resources that have contributed to the research results reported within this paper.

References

[1] Grégoire Allaire, François Jouve, Anca-Maria Toader, Structural optimization using sensitivity analysis and a level-set method, J. Comput. Phys. (2003).
[2] Jean-Louis Barrat, Glenn H. Fredrickson, Scott W. Sides, Introducing variable cell shape methods in field theory simulations of polymers, J. Phys. Chem. B 109 (14) (2005) 6694–6700, PMID: 16851752.
[3] M. Burger, S. Osher, A survey on level set methods for inverse problems and optimal design, Eur. J. Appl. Math. 16 (2005) 263–301, http://dx.doi.org/10.1017/S0956792505006182.
[4] Jean Cea, Conception optimale ou identification de formes, calcul rapide de la dérivée directionnelle de la fonction coût, ESAIM: Math. Model. Numer. Anal. 20 (3) (1986) 371–402.
[5] Tony F. Chan, Xue-Cheng Tai, Level set and total variation regularization for elliptic inverse problems with discontinuous coefficients, J. Comput. Phys. 193 (1) (2004) 40–66.
[6] Frédéric Chantalat, Charles-Henri Bruneau, Cédric Galusinski, Angelo Iollo, Level-set, penalization and Cartesian meshes: a paradigm for inverse problems and optimal design, J. Comput. Phys. 228 (17) (2009) 6291–6315.
[7] P.-G. De Gennes, A rule of sums for semidilute polymer chains near a wall, C. R. Seances Acad. Sci, Ser. B 290 (23) (1980) 509–510.
[8] M. Delfour, J. Zolésio, Shapes and Geometries, second edition, Society for Industrial and Applied Mathematics, 2011.
[9] G.H. Fredrickson, The Equilibrium Theory of Inhomogeneous Polymers, vol. 134, Oxford University Press, USA, 2006.
[10] Sharon C. Glotzer, Michael J. Solomon, Anisotropy of building blocks and their assembly into complex structures, Nat. Mater. 6 (7) (2007) 557–562.
[11] Eugene Helfand, Block copolymer theory. III. Statistical mechanics of the microdomain structure, Macromolecules 8 (4) (1975) 552–556.
[12] Eugene Helfand, Theory of inhomogeneous polymers: fundamentals of the Gaussian random walk model, J. Chem. Phys. 62 (3) (1975) 999–1005.
[13] J. Hadamard, Mémoires sur le Problème d'Analyse Relatif à l'Équilibre des Plaques Élastiques Encastrées, Oeuvre de J. Hadamard, vol. 908, C.N.R.S, Paris, 1908.
[14] Yunju La, Chiyoung Park, Tae Joo Shin, Sang Hoon Joo, Sebyung Kang, Kyoung Taek Kim, Colloidal inverse bicontinuous cubic membranes of block copolymers with tunable surface functional groups, Nat. Chem. 6 (6) (2014) 534–541.
[15] N. Laachi, K.T. Delaney, B. Kim, S.-M. Hur, R. Bristol, D. Shykind, C.J. Weinheimer, G.H. Fredrickson, The hole shrink problem: theoretical studies of directed self-assembly in cylindrical confinement, Proc. SPIE Adv. Lithogr. (2013) 868014.
[16] N. Laachi, T. Iwama, K.T. Delaney, B. Kim, R. Bristol, D. Shykind, C.J. Weinheimer, G.H. Fredrickson, Field-theoretic simulations of directed self-assembly in cylindrical confinement: placement and rectification aspects, Proc. SPIE Adv. Lithogr. (2014) 90491M.
[17] N. Laachi, H. Takahashi, K.T. Delaney, S.-M. Hur, D. Shykind, C.J. Weinheimer, G.H. Fredrickson, Self-consistent field theory of directed self-assembly in laterally confined lamellae-forming diblock copolymers, Proc. SPIE Adv. Lithogr. (2012) 83230K.
[18] Nabil Laachi, Tatsuhiro Iwama, Kris T. Delaney, David Shykind, Corey J. Weinheimer, Glenn H. Fredrickson, Directed self-assembly of linear arrays of block copolymer cylinders, J. Polym. Sci., Part B, Polym. Phys. 53 (5) (2015) 317–326.
[19] Azat Latypov, Computational solution of inverse directed self-assembly problem, in: Alternative Lithographic Technologies V, in: Proc. SPIE, vol. 8680, SPIE, 2013.
[20] Azat Latypov, Grant Garner, Moshe Preil, Gerard Schmid, Wei-Long Wang, Ji Xu, Yi Zou, Computational simulations and parametric studies for directed self-assembly process development and solution of the inverse directed self-assembly problem, Jpn. J. Appl. Phys. 53 (6S) (2014) 06JC01.
[21] M.W. Matsen, The standard Gaussian model for block copolymer melts, J. Phys. Condens. Matter 14 (2) (2002) R21.
[22] Raffaele Mezzenga, Peter Schurtenberger, Adam Burbidge, Martin Michel, Understanding foods as soft materials, Nat. Mater. 4 (10) (2005) 729–740.
[23] C. Min, F. Gibou, A second order accurate level set method on non-graded adaptive Cartesian grids, J. Comput. Phys. 225 (2007) 300–321.
[24] C. Min, F. Gibou, H. Ceniceros, A supra-convergent finite difference scheme for the variable coefficient Poisson equation on non-graded grids, J. Comput. Phys. 218 (2006) 123–140.
[25] Mohammad Mirzadeh, Arthur Guittet, Carsten Burstedde, Frederic Gibou, Parallel level-set methods on adaptive tree-based grids, J. Comp. Phys. 322 (2016) 345–364, http://dx.doi.org/10.1016/j.jcp.2016.06.017.
[26] Tri-Hung Nguyen, Tracey Hanley, Christopher J.H. Porter, Ben J. Boyd, Nanostructured liquid crystalline particles provide long duration sustained-release effect for a poorly water soluble drug after oral administration, J. Control. Release 153 (2) (2011) 180–186.

[27] S. Osher, R. Fedkiw, Level Set Methods and Dynamic Implicit Surfaces, Springer-Verlag, New York, NY, 2002.
[28] S. Osher, J.A. Sethian, Fronts propagating with curvature-dependent speed: algorithms based on Hamilton–Jacobi formulations, J. Comput. Phys. 79 (1988) 12–49.
[29] Stanley Osher, Fadil Santosa, Level set methods for optimization problems involving geometry and constraints: frequencies of a two-density inhomogeneous drum, J. Comp. Physiol. 171 (2001) 272–288.
[30] Gaddiel Y. Ouaknin, Nabil Laachi, Kris Delaney, Glenn H. Fredrickson, Frederic Gibou, Level-set strategy for inverse DSA-lithography, 2016, submitted for publication.
[31] Gaddiel Ouaknin, Nabil Laachi, Kris Delaney, Glenn H. Fredrickson, Frederic Gibou, Self-consistent field theory simulations of polymers on arbitrary domains, J. Comput. Phys. 327 (2016) 168–185.
[32] Olivier Pantz, Sensibilité de l'équation de la chaleur aux sauts de conductivité, C. R. Math. 341 (5) (2005) 333–337.
[33] Joseph Papac, Frederic Gibou, Christian Ratsch, Efficient symmetric discretization for the Poisson, heat and Stefan-type problems with Robin boundary conditions, J. Comput. Phys. 229 (3) (February 2010) 875–889.
[34] Joseph Papac, Asdis Helgadottir, Christian Ratsch, Frederic Gibou, A level set approach for diffusion and Stefan-type problems with Robin boundary conditions on quadtree/octree adaptive Cartesian grids, J. Comput. Phys. 233 (2013) 241–261.
[35] R.A. Segalman, Patterning with block copolymer thin films, Mater. Sci. Eng., R Rep. 48 (6) (2005) 191–226.
[36] R.A. Segalman, H. Yokoyama, E.J. Kramer, Graphoepitaxy of spherical domain block copolymer films, Adv. Mater. 13 (15) (2001) 1152–1155.
[37] Rachel A. Segalman, Directing self-assembly toward perfection, Science 321 (5891) (2008) 919–920.
[38] J.A. Sethian, Level Set Methods and Fast Marching Methods, Cambridge University Press, Cambridge, 1999.
[39] J. Sokolowski, J.P. Zolesio, Introduction to Shape Optimization: Shape Sensitivity Analysis, Springer Series in Computational Mathematics, Springer-Verlag, 1992.
[40] Kevin Sturm, Minimax Lagrangian approach to the differentiability of nonlinear PDE constrained shape functions without saddle point assumption, SIAM J. Control Optim. 53 (4) (2015) 2017–2039.
[41] Maxime Theillard, Landry Fokoua Djodom, Jean-Léopold Vié, Frédéric Gibou, A second-order sharp numerical method for solving the linear elasticity equations on irregular domains and adaptive grids – application to shape optimization, J. Comput. Phys. 233 (2013) 430–448.